Entanglement-enhanced lidars for simultaneous range and velocity measurements

PHYSICAL REVIEW A **96**, 040304(R) (2017)

Entanglement-enhanced lidars for simultaneous range and velocity measurements

Quntao Zhuang,[1,2,*] Zheshen Zhang,[1] and Jeffrey H. Shapiro[1]
[1]*Research Laboratory of Electronics, Massachusetts Institute of Technology, Cambridge, Massachusetts 02139, USA*
[2]*Department of Physics, Massachusetts Institute of Technology, Cambridge, Massachusetts 02139, USA*
(Received 18 May 2017; published 16 October 2017)

Lidar is a well-known optical technology for measuring a target's range and radial velocity. We describe two lidar systems that use entanglement between transmitted signals and retained idlers to obtain significant quantum enhancements in simultaneous measurements of these parameters. The first entanglement-enhanced lidar circumvents the Arthurs-Kelly uncertainty relation for simultaneous measurements of range and radial velocity from the detection of a single photon returned from the target. This performance presumes there is no extraneous (background) light, but is robust to the round-trip loss incurred by the signal photons. The second entanglement-enhanced lidar—which requires a lossless, noiseless environment—realizes Heisenberg-limited accuracies for both its range and radial-velocity measurements, i.e., their root-mean-square estimation errors are both proportional to $1/M$ when M signal photons are transmitted. These two lidars derive their entanglement-based enhancements from the use of a unitary transformation that takes a signal-idler photon pair with frequencies ω_S and ω_I and converts it to a signal-idler photon pair whose frequencies are $(\omega_S + \omega_I)/2$ and $(\omega_S - \omega_I)/2$. Insight into how this transformation provides its benefits is provided through an analogy to continuous-variable superdense coding.

DOI: 10.1103/PhysRevA.96.040304

Quantum metrology [1–3] addresses measuring unknown parameters of a physical system using quantum-mechanical resources. A typical single-parameter scenario involves interrogating a physical system with M probes that undergo independent, identical interactions with the system. These probes then carry away information that can be used to estimate the parameter of interest. When the M probes are in a product state, the standard quantum limit (SQL)—with a root-mean-square (rms) estimation error proportional to $1/\sqrt{M}$—can be achieved. Entangled probes, however, can realize the Heisenberg limit (HL) [2,3], viz., an rms estimation error that is proportional to $1/M$ [2–7]. SQL vs HL behavior for single-parameter estimation can arise, e.g., in measuring time delays [5], point-source separations [8–11], displacements [12–14], or magnetic fields [15].

Significant complications occur, in the independent, identical interactions setting, when there are multiple unknown parameters [12–15]. In particular, if these parameters are associated with noncommuting observables, then the uncertainty principle would seem to forbid obtaining unlimited simultaneous knowledge of them from a single returned probe [16–22]. In such cases, quantum-enhanced accuracy can be obtained by entangling probes with locally stored idlers [12–14,23–27], in addition to the benefit derived from entangling different probes.

In this Rapid Communication we address quantum metrology for a specific pair of parameters associated with noncommuting observables: the lidar problem of measuring both a target's range and its radial velocity. We describe two lidar systems that use entanglement between transmitted signals and retained idlers to obtain significant quantum enhancements in the simultaneous measurement of these parameters. The first circumvents the Arthurs-Kelly uncertainty relation [22] for simultaneous measurements of range and radial velocity from the detection of a single photon returned from the target. This performance presumes there is no extraneous (background) light, but is robust to the round-trip loss incurred by the signal photons. For comparison, a system that does not use entanglement would need to detect two returned signal photons to achieve the same measurement performance. Thus our system's advantage can be quite significant when the lidar-to-target-to-lidar path is very lossy. Note that it had previously been thought [28,29] that there was no entanglement advantage to be had in lossy, noiseless lidar scenarios, with Ref. [29] proving that a coherent-state probe achieves near-quantum-optimum error probability for discriminating between target absence and presence in such a case.

Our second lidar—which requires a lossless, noiseless environment—realizes HL accuracies for both its range and radial-velocity measurements, i.e., their rms errors are both proportional to $1/M$ when M signal photons are transmitted. For comparison, both the M-photon time-domain and M-photon frequency-domain Giovannetti-Lloyd-Maccone (GLM) states [5]—which also assume a lossless, noiseless operation—must probe the target to obtain the same performance without stored idlers. Thus our system's advantage can be quite significant when the probing flux must be kept as low as possible.

Lidars measure range from the round-trip time delay incurred by an optical pulse in propagating to and from the target. They measure radial velocity from the Doppler shift on the light returned from a moving target. Our lidars use time-energy entangled signal-idler photon pairs to enable joint measurements of the noncommuting observables associated with time delay and frequency shift, despite only the signal photons having interacted with the target. Moreover, our first lidar is, in essence, the $M = 1$ special case of the second, although only the first is robust to round-trip propagation loss. Both derive their entanglement-enhanced performance from the use of a two-photon unitary transformation [30,31]

*quntao@mit.edu

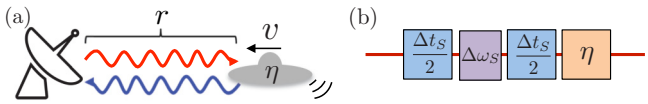

FIG. 1. (a) Lidar sensing of target range and radial velocity. η is the round-trip transmissivity, i.e., the fraction of the lidar's transmitted signal photons that return to the lidar's receiver. (b) Equivalent quantum-channel representation.

that takes a signal-idler photon pair with frequencies ω_S and ω_I and converts it to a signal-idler photon pair whose frequencies are $(\omega_S + \omega_I)/2$ and $(\omega_S - \omega_I)/2$. Interestingly, as we will show, this transformation makes our lidars behave much as continuous-variable superdense coding (CV-SDC) [32] in quantum communication, hence providing an intuitive explanation for their quantum advantage.

Lidar range and radial-velocity estimation. In our lidar sensing problem, shown in Fig. 1(a), M quasimonochromatic signal photons with a center frequency ω_{S_c} illuminate a target whose range r and radial velocity v (with $v > 0$ indicating a target moving toward the lidar) are to be estimated from the time delay, $\Delta t_S = 2r/c$, and the Doppler shift, $\Delta\omega_S = 2\omega_{S_c} v/c$, imposed on each photon that returns to the lidar, where c is light speed.

For a lidar that performs single-mode detection at its receiver, the background light at optical wavelengths can be ignored, e.g., the background light will have an average of $\sim 10^{-6}$ photons per mode in daytime operation at 1.55-μm wavelength [33]. Thus, aside from the time delay and Doppler shift incurred by each photon, the only propagation effect we shall consider for the lidar-to-target-to-lidar channel is its round-trip transmissivity η, which will typically satisfy $\eta \ll 1$, making obtaining accurate time-delay and Doppler-shift information from a small number of target-return photons a priority.

Figure 1(b) shows a channel model for the Fig. 1(a) scenario. Each signal photon incurs a time delay $\Delta t_S/2$ on its way to the target, a Doppler shift $\Delta\omega_S$ upon reflection from the target, and another $\Delta t_S/2$ time delay en route back to the lidar, where (without loss of generality) we impose the round-trip transmissivity η. In what follows, $\hat{D}_{S_t}(\Delta t_S/2)$ will denote the operator that time delays a signal photon by $\Delta t_S/2$, and $\hat{D}_{S_\omega}(\Delta\omega_S)$ will denote the operator that Doppler shifts a signal photon by $\Delta\omega_S$.

To begin our development, let us find the best that can be done when only one photon is returned from the target. Suppose that M transmitted photons are emitted one at a time by the lidar's transmitter, and that we know both those emission times *and* which transmitted photon resulted in the one returned to the lidar [34]. Because a target's range and its radial velocity are then easily calculated from that photon's time of arrival and its Doppler shift, all that follows will address limits of simultaneous time and frequency measurements. Furthermore, in our quest for quantum enhancements, we will assume that each signal photon is entangled with a retained idler photon in an initial pure state $|\psi\rangle$ and that each idler is stored, in a lossless manner [35], for a time Δt_I that is sufficient to enable its being jointly measured with its signal-photon companion should that companion be the one that is returned to the lidar.

Single-photon target-return lidar. When the lidar-to-target-to-lidar round-trip transmissivity is very low, i.e., $\eta \ll 1$, then the transmission of $M \simeq 1/\eta \gg 1$ photons is necessary for a reasonable assurance that one signal photon will be returned from that target. To minimize the M value needed to estimate the target range and radial velocity it would be best were it possible to simultaneously—and accurately—determine the time delay Δt_S and the Doppler shift $\Delta\omega_S$ from the measurement of a single returned photon. This wish would seem to violate the Arthurs-Kelly uncertainty relation [22], which states that δt_S and $\delta\omega_S$—the rms errors when time delay and Doppler shift are estimated from such a simultaneous measurement—satisfy $\delta t_S\, \delta\omega_S \geqslant 1$. However, because our lidar has the retained idler photon for use in a joint measurement with its returned-signal companion, we will see that the Arthurs-Kelly inequality can be circumvented. Indeed, starting from a biphoton state with a time-bandwidth product $TW \gg 1$ [39], we will show how $\delta t_S \simeq 1/2W$ and $\delta\omega_S \simeq 1/2T$ can be achieved simultaneously from an appropriate joint measurement.

Our single-photon lidar uses a nondegenerate spontaneous parametric downconverter (SPDC) whose output—for the signal-idler pair that will ultimately be measured—can be taken to be the biphoton state $|\psi\rangle = \int dt_S\, dt_I\, \psi(t_S,t_I)\, |t_S\rangle_S\, |t_I\rangle_I$ with the time-domain wave function given by [39]

$$\psi(t_S,t_I) \propto e^{-t_-^2/4\sigma_{\rm cor}^2 - t_+^2/4\sigma_{\rm coh}^2 - i(\Delta\omega t_-/2 + \omega_P t_+)}, \tag{1}$$

where $|t\rangle$ denotes a single photon at time t, $t_- \equiv t_S - t_I$, $t_+ \equiv (t_S + t_I)/2$, $\sigma_{\rm cor}$ is the biphoton correlation time, $\sigma_{\rm coh}$ is the pump coherence time, $\Delta\omega \equiv \omega_{S_c} - \omega_{I_c} > 0$ is the difference between the signal and idler's center frequencies, and ω_P is the pump frequency. This state's frequency-domain representation, $\int d\omega_S\, d\omega_I\, \Psi(\omega_S,\omega_I)\, |\omega_S\rangle_S\, |\omega_I\rangle_I$, where $|\omega\rangle$ denotes a single photon with frequency ω, then has the wave function

$$\Psi(\omega_S,\omega_I) \propto e^{-(\omega_- - \Delta\omega)^2\sigma_{\rm cor}^2/4 - (2\omega_+ - \omega_P)^2\sigma_{\rm coh}^2}, \tag{2}$$

with $\omega_- \equiv \omega_S - \omega_I$ and $\omega_+ \equiv (\omega_S + \omega_I)/2$.

The rms time durations of the SPDC's signal and idler photons are identical, and given by $T = \sqrt{\sigma_{\rm coh}^2 + \sigma_{\rm cor}^2/4}$. Likewise, their rms bandwidths are also identical, and given by $W = \sqrt{1/16\sigma_{\rm coh}^2 + 1/4\sigma_{\rm cor}^2}$, which we assume to be much less than $\Delta\omega$. When $\sigma_{\rm cor} = 2\sigma_{\rm coh}$, the biphoton reduces to a product of pure-state signal and idler photons satisfying $TW = 1/2$. A continuous-wave downconverter, however, typically has $\sigma_{\rm coh} \gg \sigma_{\rm cor}$ [39], so that $T \approx \sigma_{\rm coh} \gg 1/W \approx 2\sigma_{\rm cor}$, making the signal and idler highly entangled, with entanglement entropy $S_E = \log_2(2TW) \gg 1$.

Conditioned on the biphoton from Eq. (1) being the one whose returned signal and retained idler will be measured, we have that $|\psi(\boldsymbol{\theta})\rangle = \hat{D}_{S_t}(\Delta t_S/2)\hat{D}_{S_\omega}(\Delta\omega_S)\hat{D}_{S_t}(\Delta t_S/2) \otimes \hat{D}_{I_t}(\Delta t_I)|\psi\rangle$, where $\boldsymbol{\theta} = [\Delta t_S, \Delta\omega_S]^T$, with T denoting the transpose, is the state from which we will determine the signal photon's time delay and Doppler shift. Using the Cramér-Rao (CR) bound [1,40–42], we show, in Appendix A, that unbiased estimators of the signal photon's time delay and Doppler shift have rms errors that individually obey $\delta t_S \geqslant 1/2W$ and $\delta\omega_S \geqslant 1/2T$, and jointly satisfy

$$\delta t_S\, \delta\omega_S \geqslant (1 + 2TW)/8T^2W^2. \tag{3}$$

Without entanglement ($TW = 1/2$), we recover the Arthurs-Kelly inequality, but with a highly entangled signal and idler ($TW \gg 1$), we get $\delta t_S\, \delta\omega_S \geqslant 1/4TW$, which suggests that $\delta t_S = 1/2W$ and $\delta\omega_S = 1/2T$ might be realized simultaneously. We next present a theoretical design for a measurement that achieves that goal.

Our first step is to apply the biphoton unitary transformation [43],

$$\hat{B}_{SI} = \int d\omega_S \int d\omega_I \left|\frac{\omega_S+\omega_I}{2}\right\rangle_S \left|\frac{\omega_S-\omega_I}{2}\right\rangle_I {}_S\langle\omega_S|\,{}_I\langle\omega_I| = \int dt_S \int dt_I\, |t_S+t_I\rangle_S\, |t_S-t_I\rangle_I\, {}_S\langle t_S|\,{}_I\langle t_I|\,, \tag{4}$$

to the postselected state $|\psi(\boldsymbol{\theta})\rangle$ to obtain the product state $\hat{B}_{SI}|\psi(\boldsymbol{\theta})\rangle = |\psi_S(\boldsymbol{\theta})\rangle_S \otimes |\psi_I(\boldsymbol{\theta})\rangle_I$, where, assuming $\sigma_{\rm coh} \gg \sigma_{\rm cor}$, we have that

$$|\psi_S(\boldsymbol{\theta})\rangle_S \propto \int d\omega_S\, e^{i(\omega_S+\Delta\omega)(\Delta t_S+\Delta t_I)-(2\omega_S-\omega_P-\Delta\omega_S)^2T^2}\, |\omega_S\rangle_S\,, \tag{5}$$

and

$$|\psi_I(\boldsymbol{\theta})\rangle_I \propto \int dt_I\, e^{-i(\Delta\omega_S+\Delta\omega)t_I/2-(t_I-\Delta t_S+\Delta t_I)^2W^2}\, |t_I\rangle_I\,. \tag{6}$$

Next, we measure the single-photon frequency observable of the signal photon and the single-photon arrival-time observable of the idler photon, i.e., $\hat{\omega}_S = \int d\omega_S\, \omega_S |\omega_S\rangle_{SS}\langle\omega_S|$ and $\hat{t}_I = \int dt_I\, t_I |t_I\rangle_{II}\langle t_I|$. Using the resulting outcomes, $\tilde{\omega}_S$ and $\tilde{t}_I$, we generate our time-delay and Doppler-shift estimates $\widetilde{\Delta t_S} = \tilde{t}_I + \Delta t_I$ and $\widetilde{\Delta\omega_S} = 2\tilde{\omega}_S - \omega_P$. These estimates are unbiased, $\langle\widetilde{\Delta t_S}\rangle = \Delta t_S$ and $\langle\widetilde{\Delta\omega_S}\rangle = \Delta\omega_S$, with standard deviations $1/2W$ and $1/2T$, thus showing that our entanglement-enhanced lidar *simultaneously* realizes the CR bounds on δt_S and $\delta\omega_S$ from a single-photon target return.

Connection to CV-SDC. Figure 2 shows entangled-state and product-state representations of our single-photon lidar for the photon pair that is ultimately measured. In Fig. 2(a), we start from a signal-idler (S-I) product state whose frequency-domain wave function is proportional to $e^{-(2\omega_S-\omega_P)^2\sigma_{\rm coh}^2-(2\omega_I-\Delta\omega)^2\sigma_{\rm cor}^2/4}$. Applying the single-photon unitary transformation $\hat{B}_{SI}^\dagger$ to this state then yields the biphoton state from Eq. (1), although in experiments we start from the biphoton state in Eq. (1) directly. After that biphoton undergoes the time delays and Doppler shift shown in Fig. 2(a), the application of $\hat{B}_{SI}$ converts them back to a product state, from which a signal-photon frequency measurement $\tilde{\omega}_S$ and an idler-photon arrival-time measurement $\tilde{t}_I$ provide the information needed for simultaneous Doppler-shift and time-delay estimates. The product-state source output to product-state measurement input is thus governed by the single-photon unitary transformation

$$\hat{U} \equiv \hat{B}_{SI}\big[\hat{D}_{S_t}(\Delta t_S/2)\hat{D}_{S_\omega}(\Delta\omega_S)\hat{D}_{S_t}(\Delta t_S/2) \otimes \hat{D}_{I_t}(\Delta t_I)\big]\hat{B}_{SI}^\dagger. \tag{7}$$

After simple algebra, $\hat{U}$ can be rewritten—up to a global phase—as shown in Fig. 2(b):

$$\hat{U} = \big[\hat{D}_{S_t}(\Delta t_S+\Delta t_I)\hat{D}_{S_\omega}(\Delta\omega_S/2)\big] \otimes \big[\hat{D}_{I_t}(\Delta t_S-\Delta t_I)\hat{D}_{I_\omega}(\Delta\omega_S/2)\big]. \tag{8}$$

This form of $\hat{U}$ acting directly on the same signal-idler product state that was the input in Fig. 2(a) immediately leads to our single-photon lidar's being able to sense the Doppler shift from a signal-photon measurement and arrival time from an idler-photon measurement.

The preceding $\hat{U}$ representations bear a clear similarity to CV-SDC [32]. In CV-SDC, Alice initially prepares quadrature-entangled signal and idler beams with average photon numbers $\bar{n} \gg 1$, then sends the idler to Bob while retaining the signal. Next, Alice displaces her signal beam's two quadratures with her analog messages and sends that modulated beam to Bob. Bob combines Alice's modulated signal with his retained idler on a 50-50 beam splitter to recover a product of displaced squeezed-vacuum states from which he can obtain Alice's messages (with a pair of homodyne detectors) at a capacity double that of coherent-state communication with an average photon number $\bar{n}$. CV-SDC's continuous-variable entanglement preparation, encoding, and product-state recovery are analogous to the $\hat{B}_{SI}^\dagger$ time delays and Doppler shift, and $\hat{B}_{SI}$ transformations in Fig. 2(a).

Lidar with simultaneous HL scaling. Giovannetti, Lloyd, and Maccone showed [5] that when the M-photon, M-mode, frequency-domain GLM signal state, $|\psi\rangle_{S_\omega} \propto \int d\omega_S\, e^{-\omega_S^2/4W^2} \otimes_{m=1}^M |\omega_S\rangle_{S_m}$, interrogates a perfectly reflecting target, then time-resolved detection of all M photons in the absence of background noise enables the target's round-trip time delay Δt_S to be estimated with HL rms accuracy $\delta t_S = 1/2MW$. Likewise, the M-photon, M-mode, time-domain GLM signal state, $|\psi\rangle_{S_t} \propto \int dt_S\, e^{-t_S^2/4T^2} \otimes_{m=1}^M |t_S\rangle_{S_m}$, enables that target's Doppler shift $\Delta\omega_S$ to be estimated with HL rms accuracy $\delta\omega_S = 1/2MT$ in this lossless and noiseless scenario. These measurements are an either-or proposition: If an M-photon GLM state interrogates the target, we cannot get both $\delta t_S = 1/2MW$ and $\delta\omega_S = 1/2MT$. By sending an $M/2$-photon, frequency-domain GLM state, followed by an $M/2$-photon, time-domain GLM state, time-delay and Doppler-shift measurements with $\delta t_S = 1/MW$ and $\delta\omega_S = 1/MT$ can be obtained, but our second lidar will realize $\delta t_s = 1/2MW$ and $\delta\omega_S = 1/2MT$ from the transmission of M signal photons.

To simultaneously achieve HL accuracies, we employ two GLM states together with the M-mode generalization of our first lidar's $\hat{U}$ transformation (see Fig. 3). We start from GLM

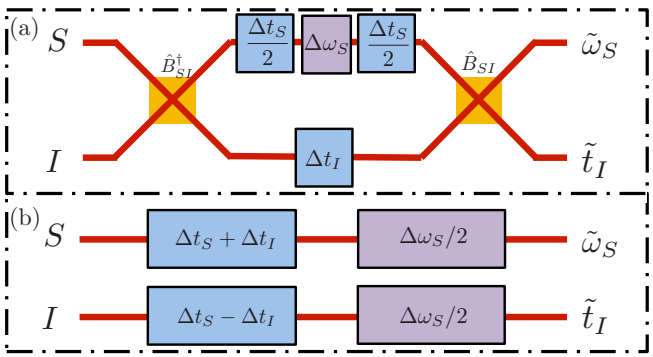

FIG. 2. (a) Entangled-state and (b) product-state representations of the single-photon target-return lidar.

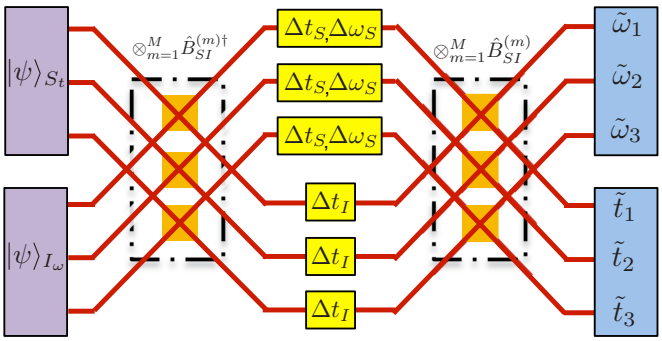

FIG. 3. Schematic for simultaneous time-delay and Doppler-shift measurements with HL rms accuracies ($M = 3$).

signal and idler states $|\psi\rangle_{S_t}$ and $|\psi\rangle_{I_\omega}$ that are entangled by the application of $\otimes_{m=1}^{M}\hat{B}_{SI}^{(m)\dagger}$. Next, the signal photons illuminate and return from the target, having accumulated a round-trip delay Δt_S and a Doppler shift $\Delta\omega_S$, while the idler photons are stored at the lidar for a time Δt_I. Applying $\otimes_{m=1}^{M}\hat{B}_{SI}^{(m)}$ to the returned and retained photons then undoes the entanglement. Paralleling the development of Eq. (8), we find that the state transformation for this arrangement is

$$\hat{U}_M = \left[\otimes_{m=1}^{M}\hat{D}_{S_{t_m}}(\Delta t_S + \Delta t_I)\hat{D}_{S_{\omega_m}}(\Delta\omega_S/2)\right] \otimes \left[\otimes_{m=1}^{M}\hat{D}_{I_{t_m}}(\Delta t_S - \Delta t_I)\hat{D}_{I_{\omega_m}}(\Delta\omega_S/2)\right]. \quad (9)$$

It now follows that a Doppler shift measurement on the $\hat{U}_M$-transformed signal photons has an rms accuracy $\delta\omega_S = 1/2MT$ and a time-delay measurement on the $\hat{U}_M$-transformed idler photons has an rms accuracy $1/2MW$.

Discussion. We have exhibited lidars that provide entanglement-enhanced accuracies in the simultaneous measurements of target range and radial velocity. These parameters are associated with noncommuting observables: a single photon's arrival time and frequency. Our general scheme of transforming operations with noncommuting generators to commuting observables can be applied to other simultaneous-measurement scenarios that involve noncommuting generators.

Two final items deserve discussion: idler storage loss and realizing the $\hat{B}_{SI}$ transformation. Loss of a single idler photon kills the performance gain of our GLM-based lidar over an unentangled system, but idler storage loss has a more benign impact on our single-photon lidar. Lossless idler storage enables our lidar to make simultaneous time-delay (range) and frequency-shift (radial-velocity) measurements at their *individual* CR-bound limits from the detection of *one* signal photon, an event that occurs with success probability η. Without entanglement, however, *two* signal photons must be received to achieve this performance, an event that occurs with success probability η^2. When our single-photon lidar has an overall idler storage efficiency η_I, its success probability is $\eta_I\eta$. Consider idler storage in a short fiber-loop memory. Such a memory could be loaded and unloaded with an optically controlled directional coupler. A portion of the pump pulse for Alice's SPDC could gate that coupler to load the idler photon into the memory, and—if the coupler could be arranged to have single-photon sensitivity—the returned signal photon could gate the coupler to unload the memory's stored idler photon. A target at a 37.5-km range would then require 50 km of recirculating fiber propagation. With 0.2-dB/km fiber loss, that would imply $\eta_I = 0.1$. So, for $\eta \ll 0.1$, as could well be the case, our lidar would enjoy a substantial performance advantage despite its 10-dB idler storage loss.

We have been exploring how $\hat{B}_{SI}$ might be realized using single-photon $\chi^{(2)}$ interactions and linear optics [44–48]. Our notional scheme, for approximating it over the bandwidth occupied by the returned signal and retained idler's biphoton state, is shown in Appendix B. It uses single-photon-sensitive SPDCs to convert single photons at frequencies ω_S and ω_I to orthogonally polarized photon pairs at frequencies $\omega_S/2$ and $\omega_I/2$. One photon from each pair is then applied to a single-photon-sensitive sum-frequency generator and a single-photon-sensitive difference-frequency generator to produce outputs at $(\omega_S + \omega_I)/2$ and $(\omega_S - \omega_I)/2$.

Acknowledgments. This research was supported by Air Force Office of Scientific Research Grant No. FA9550-14-1-0052. Q.Z. acknowledges support from the Claude E. Shannon Research Assistantship.

APPENDIX A: TIME-FREQUENCY CRAMÉR-RAO BOUND

Let the positive operator-valued measurement $\hat{\Pi}_{\tilde{\boldsymbol{\theta}}}$ on the postselected state $|\psi(\boldsymbol{\theta})\rangle$ be an unbiased estimator of $\boldsymbol{\theta}$. The CR bound [42] on this estimator's error-covariance matrix, $\mathbf{V}(\boldsymbol{\theta}) = \langle(\tilde{\boldsymbol{\theta}} - \boldsymbol{\theta})(\tilde{\boldsymbol{\theta}} - \boldsymbol{\theta})^T\rangle$, is

$$\mathrm{tr}[\mathbf{G}\mathbf{V}(\boldsymbol{\theta})] \geqslant \mathrm{tr}\left[\mathbf{G}\mathbf{J}_{\boldsymbol{\theta}}^{-1}\right] + \left[\sqrt{\det(\mathbf{G})}/\det(\mathbf{J}_{\boldsymbol{\theta}})\right] \times |\langle\psi(\boldsymbol{\theta})|\left[L_{\Delta t_S}, L_{\Delta\omega_S}\right]|\psi(\boldsymbol{\theta})\rangle|,$$

where $\mathbf{G}$ is an arbitrary 2×2 positive-semidefinite real-valued cost matrix; $\det(\cdot)$ denotes the determinant; $[\hat{a},\hat{b}]$ denotes the commutator $\hat{a}\hat{b} - \hat{b}\hat{a}$; $\mathbf{J}_{\boldsymbol{\theta}}$ is the quantum Fisher-information matrix, whose jkth element, for $j,k = \Delta t_S, \Delta\omega_S$, is $(\mathbf{J}_{\boldsymbol{\theta}})_{jk} \equiv 4[\mathrm{Re}(\partial_{\theta_j}\langle\psi(\boldsymbol{\theta})|\partial_{\theta_k}|\psi(\boldsymbol{\theta})\rangle) + \langle\psi(\boldsymbol{\theta})|\partial_{\theta_j}|\psi(\boldsymbol{\theta})\rangle\langle\psi(\boldsymbol{\theta})|\partial_{\theta_k}|\psi(\boldsymbol{\theta})\rangle]$; and, for $j = \Delta t_S, \Delta\omega_S$, $L_j \equiv 2(\partial_{\theta_j}|\psi(\boldsymbol{\theta})\rangle\langle\psi(\boldsymbol{\theta})| + |\psi(\boldsymbol{\theta})\rangle\partial_{\theta_j}\langle\psi(\boldsymbol{\theta})|)$ are the symmetric logarithmic derivatives.

The time-domain wave function of $|\psi(\boldsymbol{\theta})\rangle$ is $\psi_{\boldsymbol{\theta}}(t_S,t_I) = \psi(t_S - \Delta t_S, t_I - \Delta t_I)e^{-i\Delta\omega_S(t_S - \Delta t_S/2)}$, from which we obtain $\mathbf{J}_{\boldsymbol{\theta}} = 4\,\mathrm{diag}[W^2,T^2]$, and $|\langle\psi(\boldsymbol{\theta})|[L_{\Delta t_S}, L_{\Delta\omega_S}]|\psi(\boldsymbol{\theta})\rangle| = 4$. Next, using $G = \mathrm{diag}[1,0]$ and $\mathrm{diag}[0,1]$ in the CR bound, we get $\delta t_S \geqslant 1/2W$ and $\delta\omega_S \geqslant 1/2T$. Maximizing the CR bound for $G = \mathrm{diag}[W^2, zT^2]$ over $z \geqslant 0$ then gives (3):

$$\delta t_S^2\,\delta\omega_S^2 \geqslant \frac{\delta\omega_S^2}{W^2}\left(\frac{1}{4} + \frac{1}{16T^2W^2\left(4T^2\delta\omega_S^2 - 1\right)}\right) \geqslant (1 + 2TW)^2/64T^4W^4.$$

APPENDIX B: APPROXIMATING $\hat{B}_{SI}$

Figure 4 depicts a notional scheme for approximating the biphoton unitary transform $\hat{B}_{SI}$ over the bandwidth occupied by the joint state $|\psi(\boldsymbol{\theta})\rangle$. The SPDCs are type-II phase matched and satisfy the extended phase-matching condition [49] over an appropriately broad bandwidth, and they are presumed to have 100% conversion efficiency for single-photon pumps. Thus a frequency-ω_S signal photon arriving at the upper

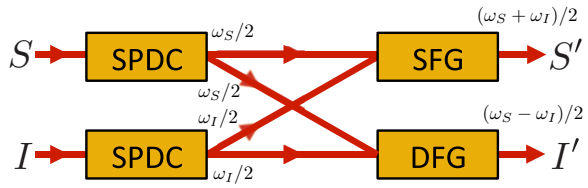

FIG. 4. Notional scheme for approximating the biphoton transform $\hat{B}_{SI}$. SPDC: Single-photon-sensitive spontaneous parametric downconverter with extended phase matching. SFG: Single-photon-sensitive sum-frequency generator. DFG: Single-photon-sensitive difference-frequency generator.

SPDC in Fig. 4 is converted into a pair of orthogonally polarized frequency-$\omega_S/2$ photons, and a frequency-ω_I idler photon arriving at the lower SPDC in Fig. 4 is converted into a pair of orthogonally polarized frequency-$\omega_I/2$ photons. Polarizing beam splitters (not shown in Fig. 4) then direct one frequency-$\omega_S/2$ photon and one frequency-$\omega_I/2$ photon to a sum-frequency generator (SFG) [50] and the other frequency-$\omega_S/2$ and frequency-$\omega_I/2$ photons to a difference-frequency generator (DFG) realized by four-wave mixing with a strong pump beam [51,52]. Both the SFG and DFG are presumed to have 100% conversion efficiency at the single-photon level over an appropriately broad bandwidth. Their respective outputs are thus single photons at frequencies $(\omega_S+\omega_I)/2$ and $(\omega_S-\omega_I)/2$.

The SPDC and SFG blocks in Fig. 4 require single-photon-sensitive $\chi^{(2)}$ interactions [46–48], such as those previously considered for use in quantum computation [45] and optimum mixed-state discrimination [53]. The DFG block in Fig. 4 employs four-wave mixing with a strong (hence classical) pump, which makes it effectively a single-photon-sensitive $\chi^{(2)}$ interaction. Thus our notional scheme for realizing the $\hat{B}_{SI}$ transformation only requires single-photon-sensitive $\chi^{(2)}$ interactions and linear optics.

[1] C. W. Helstrom, *Quantum Detection and Estimation Theory* (Academic Press, New York, 1976).
[2] V. Giovannetti, S. Lloyd, and L. Maccone, Phys. Rev. Lett. **96**, 010401 (2006).
[3] V. Giovannetti, S. Lloyd, and L. Maccone, Nat. Photon. **5**, 222 (2011).
[4] M. Zwierz, C. A. Pérez-Delgado, and P. Kok, Phys. Rev. Lett. **105**, 180402 (2010).
[5] V. Giovannetti, S. Lloyd, and L. Maccone, Nature (London) **412**, 417 (2001).
[6] V. Giovannetti, S. Lloyd, and L. Maccone, Science **306**, 1330 (2004).
[7] B. Escher, R. de Matos Filho, and L. Davidovich, Nat. Phys. **7**, 406 (2011).
[8] R. Nair and M. Tsang, Phys. Rev. Lett. **117**, 190801 (2016).
[9] C. Lupo and S. Pirandola, Phys. Rev. Lett. **117**, 190802 (2016).
[10] M. Tsang, R. Nair, and X.-M. Lu, Phys. Rev. X **6**, 031033 (2016).
[11] R. Kerviche, S. Guha, and A. Ashok, arXiv:1701.04913.
[12] M. G. Genoni, M. G. A. Paris, G. Adesso, H. Nha, P. L. Knight, and M. S. Kim, Phys. Rev. A **87**, 012107 (2013).
[13] S. Steinlechner, J. Bauchrowitz, M. Meinders, H. Müller-Ebhardt, K. Danzmann, and R. Schnabel, Nat. Photon. **7**, 626 (2013).
[14] M. Ast, S. Steinlechner, and R. Schnabel, Phys. Rev. Lett. **117**, 180801 (2016).
[15] T. Baumgratz and A. Datta, Phys. Rev. Lett. **116**, 030801 (2016).
[16] K. Fujikawa, Int. J. Mod. Phys. A **29**, 1450016 (2014).
[17] M. Ozawa, Phys. Rev. A **67**, 042105 (2003).
[18] K. Fujikawa, Phys. Rev. A **85**, 062117 (2012).
[19] W. Heisenberg, Z. Phys. **43**, 172 (1927).
[20] E. H. Kennard, Z. Phys. **44**, 326 (1927).
[21] H. P. Robertson, Phys. Rev. **34**, 163 (1929).
[22] E. Arthurs and J. Kelly, Bell Syst. Tech. J. **44**, 725 (1965).
[23] M. A. Ballester, Phys. Rev. A **70**, 032310 (2004).
[24] D. G. Fischer, H. Mack, M. A. Cirone, and M. Freyberger, Phys. Rev. A **64**, 022309 (2001).
[25] A. Fujiwara, Phys. Rev. A **63**, 042304 (2001).
[26] A. Fujiwara and H. Imai, J. Phys. A **36**, 8093 (2003).
[27] M. A. Ballester, Phys. Rev. A **69**, 022303 (2004).
[28] H. P. Yuen and R. Nair, Phys. Rev. A **80**, 023816 (2009).
[29] R. Nair, Phys. Rev. A **84**, 032312 (2011).
[30] M. Fiorentino and F. N. C. Wong, Phys. Rev. Lett. **93**, 070502 (2004).
[31] B. Hacker, S. Welte, G. Rempe, and S. Ritter, Nature (London) **536**, 193 (2016).
[32] S. L. Braunstein and H. J. Kimble, Phys. Rev. A **61**, 042302 (2000).
[33] J. H. Shapiro, S. Guha, and B. I. Erkmen, J. Opt. Netw. **4**, 501 (2005).
[34] The lidar transmitter will employ an SPDC source with a repetitively pulsed pump laser. Each signal-idler pair emission then coincides with the occurrence of a pump pulse. By choosing the source's pulse-repetition time to exceed the round-trip time delay to the maximum target range of interest, any returned signal photon must be due to the most recently transmitted signal pulse.
[35] A low-loss optical fiber is currently the best quantum memory for storing a ∼THz-bandwidth, 1.55-μm-wavelength idler pulse. Such a memory would not be lossless, but initial assessments of quantum-enhanced sensors have frequently assumed lossless equipment (see, e.g., the initial descriptions of optical-frequency quantum illumination [36,37]). Moreover, recent work on photonic quantum memory [38] could ultimately lead to lower-loss storage than an optical fiber.
[36] S. Lloyd, Science **321**, 1463 (2008).
[37] S.-H. Tan, B. I. Erkmen, V. Giovannetti, S. Guha, S. Lloyd, L. Maccone, S. Pirandola, and J. H. Shapiro, Phys. Rev. Lett. **101**, 253601 (2008).
[38] D. G. England, K. A. G. Fisher, J.-P. W. MacLean, P. J. Bustard, R. Lausten, K. J. Resch, and B. J. Sussman, Phys. Rev. Lett. **114**, 053602 (2015).
[39] Z. Zhang, J. Mower, D. Englund, F. N. C. Wong, and J. H. Shapiro, Phys. Rev. Lett. **112**, 120506 (2014).

[40] A. Holevo, *Probabilistic and Statistical Aspects of Quantum Mechanics* (North-Holland, Amsterdam, 1982).

[41] H. P. Yuen and M. Lax, IEEE Trans. Inf. Theory **19**, 740 (1973).

[42] A. Fujiwara, University of Tokyo Mathematical Engineering Technical Report No. METR 94-09, 1994 (unpublished).

[43] For brevity, we have omitted the time delays that are needed to make this transformation causal. Assuming a nondegenerate SPDC ensures that both post-$\hat{B}_{SI}$ photons will be at optical frequencies.

[44] M. Y. Niu, B. C. Sanders, F. N. C. Wong, and J. H. Shapiro, Phys. Rev. Lett. **118**, 123601 (2017).

[45] M. Y. Niu, I. L. Chuang, and J. H. Shapiro, arXiv:1704.03431.

[46] L. K. Shalm, D. R. Hamel, Z. Yan, C. Simon, K. J. Resch, and T. Jennewein, Nat. Phys. **9**, 19 (2013).

[47] T. Guerreiro, E. Pomarico, B. Sanguinetti, N. Sangouard, J. S. Pelc, C. Langrock, M. M. Fejer, H. Zbinden, R. T. Thew, and N. Gisin, Nat. Commun. **4**, 2324 (2013).

[48] T. Guerreiro, A. Martin, B. Sanguinetti, J. S. Pelc, C. Langrock, M. M. Fejer, N. Gisin, H. Zbinden, N. Sangouard, and R. T. Thew, Phys. Rev. Lett. **113**, 173601 (2014).

[49] V. Giovannetti, L. Maccone, J. H. Shapiro, and F. N. C. Wong, Phys. Rev. Lett. **88**, 183602 (2002).

[50] Y. Sasaki and Y. Ohmori, Appl. Phys. Lett. **39**, 466 (1981).

[51] K. Inoue and H. Toba, IEEE Photon. Technol. Lett. **4**, 69 (1992).

[52] J. Zhou, N. Park, K. J. Vahala, M. A. Newkirk, and B. I. Miller, IEEE Photon. Technol. Lett. **6**, 984 (1994).

[53] Q. Zhuang, Z. Zhang, and J. H. Shapiro, Phys. Rev. Lett. **118**, 040801 (2017).